Int. J. Heat Mass Transfer. Vol. 15, pp. 73–90. Pergamon Press 1972. Printed in Great Britain

TRANSIENT THREE-DIMENSIONAL NATURAL CONVECTION IN CONFINED POROUS MEDIA

P. H. HOLST† and K. AZIZ
The University of Calgary, Calgary, Alberta, Canada

(*Received* 15 *April* 1971)

Abstract—Experimental investigations of natural convection in a confined porous medium have shown that motion may be two-dimensional or three-dimensional. The mode of the convection is dependent on the physical configuration and the Rayleigh number. This paper deals with the theoretical results obtained from the finite difference solution of the equations describing transient natural convection in porous media. The equations had been made more amenable to a numerical solution by introducing a vector potential, which may be regarded as the three-dimensional counterpart of the stream function.

Numerical results indicate that under certain conditions three-dimensional motion would result in significantly higher heat transfer rates across the porous medium than two-dimensional motion at the same Rayleigh number. The convection pattern of the three-dimensional motion is illustrated by isometric projections of isothermal surfaces and streaklines which trace the path of a fluid particle. The linearized equations are solved to provide an estimate of the number of possible convective modes as a function of the Rayleigh number.

NOMENCLATURE

A, aspect ratio (dimensionless) $= L_z/L_x$;
B, aspect ratio (dimensionless) $= L_z/L_y$;
C_p, heat capacity [$m^2/s^2°C$];
g, gravitational acceleration $= 9.807\,m/s^2$;
G, gravity vector as defined by equation (4);
K, permeability [m^2];
L, physical length in direction of subscript [m];
l, vertical wave number as defined by equation (46);
m, horizontal wave number (y-direction) as defined by equation (46);
n, horizontal wave number (z-direction) as defined by equation (46);
Nu, Nusselt number $= \left| \int_0^1 \int_0^1 \left. \frac{\partial T}{\partial \bar{x}} \right|_{x=0} d\bar{z} d\bar{y} \right|$;
P, pressure;
R, Rayleigh number as defined by equation (18);
t, $t \cdot t^* =$ time [s];
t^*, time constant $= [L_z^2(\rho C_p)_m/\lambda_m]$ [s^{-1}];
T, $T_0 + \Delta T_0 \bar{T} =$ temperature [°C];
ΔT_0, temperature gradient across porous media;
w, superficial mass flux [kg/m^2];
w_x^*, constant defined by equation (33);
x,y,z, coordinate axis as defined in Fig. 1.

Greek letters

β, coefficient of thermal expansion [$°C^{-1}$];
$\Delta x, \Delta y, \Delta z$, grid spacing in the x,y,z direction;
Δt, time step;
∇, Del operator $= \frac{\partial}{\partial x}, \frac{\partial}{\partial y}, \frac{\partial}{\partial z}$;
∇^2, Laplacian operator $= \frac{\partial^2}{\partial x^2} + \frac{\partial^2}{\partial y^2} + \frac{\partial^2}{\partial x^2}$;

† Present address, Mobil Oil Canada, Ltd.

$\bar{\nabla}$, $A^2 \frac{\partial^2}{\partial \bar{x}^2} + B^2 \frac{\partial^2}{\partial \bar{y}^2} + \frac{\partial^2}{\partial \bar{z}^2}$:

∇_1^2, $\frac{\partial^2}{\partial y^2} + \frac{\partial^2}{\partial z^2}$:

$\bar{\nabla}_1^2$, $B^2 \frac{\partial^2}{\partial \bar{y}^2} + \frac{\partial^2}{\partial \bar{z}^2}$:

θ, angle of inclination (cf. Fig. 1);
ρ, density [kg/m^3];
λ, thermal conductivity [kgm/°Cs^3];
μ, fluid viscosity [kg/ms];
ϕ, porosity (fraction);
Ξ, vorticity, ξ_1, ξ_2, ξ_3, cf. equation (19);
ω, relaxation factor, cf. equation (A.4);
Ω, operator as defined by equations (A.8)–(A.10);
ε, allowable error;
$\boldsymbol{\psi}$, vector potential, ψ_1, ψ_2, ψ_3, cf. equation (21).

Subscripts

c, critical;
f, fluid;
i,j,k, grid point;
m, solid–fluid mixture;
n, time level;
o, at cold surface temperature;
p, perturbation from conduction;
s, solid;
x,y,z, in direction of x,y,z;
CD, conduction.

Superscripts

v, iteration level;
$-$, dimensionless quantity.

In some instances the subscript f has been omitted in order to avoid double subscripting. Thus ρ_0 is equivalent to ρ_{f_0}.

1. INTRODUCTION

A VISCOUS fluid initially at rest will exhibit motion when heated from below if and only if the newly established buoyancey forces are of sufficient magnitude to overcome the viscous retardation of the fluid. Rayleigh [1] investigated this problem theoretically by writing the appropriate mass, momentum and energy balances on a differential volume of fluid. After a series of simplifications he arrived at a criterion predicting the onset of convection for a hypothetical case of a horizontal fluid layer with upper and lower surfaces free. He also derived a dimensionless group, subsequently named the Rayleigh [1] number, which determined the onset and the magnitude of the convective motions. Since the pioneering work of Rayleigh more realistic problems have been investigated. Chandrasekhar [2], Aziz [3] and Roberts [4] may be consulted for reviews of more recent developments.

When the fluid saturates a porous medium, which in turn is heated from below, the same physical process takes place. Lapwood [5] was one of the early investigators to recognize this. Applying essentially the same procedure as employed by Rayleigh [1], Lapwood derived the mass, momentum and energy balances for the system. Neglecting the temperature dependence of the fluid and media properties (except where they create buoyancy), and any nonlinear terms in the equations, Lapwood arrived at a solution, which due to the nature of the assumptions was valid only at the point of impending fluid motion. Subsequent investigators (Wooding [6, 17], Elder [7, 8], Karra [9], Chan *et al.* [10]) did not neglect the nonlinear terms in the governing equations, and obtained steady state and in some instances transient two-dimensional numerical solutions.

Considering a physical situation of relatively small dimensions, i.e. height to depth ratio in the order of unity, the natural convection induced by the rising, heated, fluid may be of two forms. The first type requires the motion of two opposing vertical surfaces, to be in the same direction. In this case convection would most likely be in the form of two-dimensional rolls.† The other possibility has the motion at two opposing

† The possibility of 3-D motion is determined by the critical Rayleigh number for the motion, which in most instances is high.

surfaces in opposite directions. In this case convection would be cellular or three-dimensional. In many practical applications, conditions are such that cellular motion would be physically preferred and consequently existing solutions would not be applicable.

An aspect of immediate concern to the authors was the design of experimental equipment to substantiate the mathematical solution for natural convection in porous media. The experimental investigation was to be and has subsequently been done (Holst [11]) employing thermistor probes to monitor the temperature distribution in a porous medium heated from below as a function of time. As the number of temperature probes required to adequately monitor three-dimensional motion is excessive, the design of the system had to be such that only two-dimensional motion is induced under a wide range of external conditions. Of secondary interest was the effect of the three-dimensional motion on the heat transfer characteristics of the medium.

Based on this need of a three-dimensional solution, the physical system was modelled mathematically by writing mass and energy balances on a differential volume of a porous medium. Darcy's law was employed as the force balance. The equations were simplified by neglecting the temperature dependence of the fluid properties (except where density changes create buoyancy). First, the equations were linearized and solved to obtain the critical Rayleigh number as a function of the physical dimensions of the porous medium. Subsequently the nonlinear equations were solved by finite difference methods. In order to obtain a reasonably efficient solution, the equations were formulated in terms of a vector potential, the three-dimensional analog of the stream function. This formulation was found to be highly advantageous by one of the authors (Aziz and Hellums [12]) in the related problem of natural convection in an open cavity.

In this paper only a brief reference is made to two-dimensional studies and experimental work. These aspects of the problem are presented elsewhere (Holst and Aziz [13]).

2. MATHEMATICAL FORMULATION

Figure 1 represents a porous medium tilted at an angle θ with the vertical. The physical system can be modelled by writing the appropriate mass,

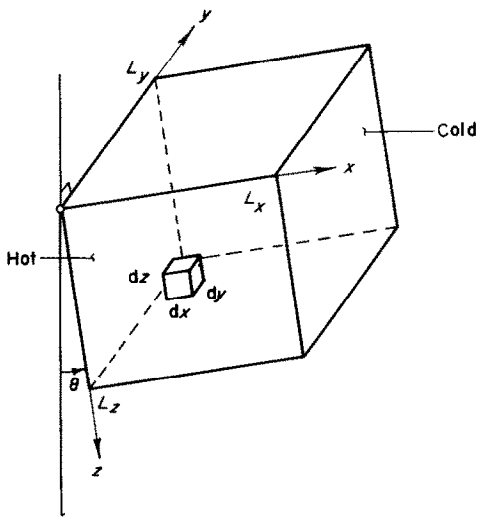

FIG. 1. The physical system as modelled mathematically.

energy and momentum balances on the differential volume also shown in Fig. 1. The mass balance for an incompressible system is given by

$$\nabla . w = 0 \tag{1}$$

The energy balance, subject to the assumptions stated later is given by (e.g. Prats [14])

$$\nabla^2 T - \frac{C_{pf}}{\lambda_m} w . \nabla T = \frac{(\rho C_p)_m}{\lambda_m} \frac{\partial T}{\partial t}. \tag{2}$$

The assumptions employed in deriving equation (2) are: fluid and porous medium properties are independent of temperature and pressure, except where a density change creates buoyancy; heat effects due to viscous dissipation are negligible; the fluid and porous medium may be combined and treated as a homogeneous mass when considering conduction. These assumptions are reasonable if the temperature gradient to which

the porous medium is subjected is reasonable and the effective thermal conductivity of the solid–fluid mixture is measured for the combination. They are the assumptions normally made in formulating the mathematical analog of natural convection problems.

The momentum balance for the porous medium is stated in the form of Darcy's law:

$$\boldsymbol{w} = -\frac{K\rho_f}{\mu}[\nabla P + \boldsymbol{G}] \tag{3}$$

where

$$\boldsymbol{G} = (\rho_f g \sin\theta, 0, -\rho_f g \cos\theta). \tag{4}$$

Equations (1)–(3) were solved subject to the following initial and boundary conditions.

Initial conditions. The temperature distribution is a prescribed function of the space coordinates. Normally it was assumed to be equal to the temperature of the cold surface. The mass flux distribution was taken to be consistent with the temperature distribution, normally equal to zero.

Boundary conditions. Two opposing surfaces ($x = 0$ and $x = L_x$) were kept at a constant temperature. The surface at $x = 0$ being kept at a higher temperature than the opposing surface. The remaining sides were perfectly insulated. No fluid was allowed to flow out of the system. Equations (1)–(3) may be solved subject to some additional assumptions. In what follows the linearized version of the equations are formulated first. The solution to these equations may be employed to establish the critical Rayleigh number, i.e. the minimum vertical temperature gradient for which natural convection will be sustained in a porous medium. As a critical Rayleigh number exists only in a horizontal system, the following development implies such a horizontal system ($\theta = 90°$).

(a) *Linear equations*

It is convenient to look at temperature and pressure as

$$T = T_{CD} + T_p \tag{5}$$

$$P = P_{CD} + P_p. \tag{6}$$

In addition we need an equation of state for the fluid. For our work we choose the usual first order relationship:

$$\rho_f = \rho_0(1 - \beta(T - T_0)]. \tag{7}$$

The subscript CD denotes the conduction solution which is obtained when the Rayleigh number is zero, while the subscript p denotes the perturbation solution.

The steady state conduction solution, subject to the boundary condition stated previously, is given by:

$$T_{CD} = T_0 + \Delta T_0 x/L_x \tag{8}$$

$$P_{CD} = P_0 - \rho_{f_{C_0}} x \tag{9}$$

$$\boldsymbol{w}_{CD} = 0. \tag{10}$$

Combining equations (8), (5) and (2) yields after neglecting all non-linear terms:

$$\nabla^2 T_p - \frac{C_{pf}}{\lambda_m}\frac{\Delta T_0}{L_x} w_x = \frac{(\rho C_p)_m}{\lambda_m}\frac{\partial T_p}{\partial t}. \tag{11}$$

Equation (3), the equation of motion may similarly be rewritten to yield:

$$\boldsymbol{w} = -\frac{K\rho_f}{\mu}(\nabla P_p + \boldsymbol{G}_p) \tag{12}$$

where

$$\boldsymbol{G}_p = \boldsymbol{G}_h + \nabla P_{CD} = [(\rho_f - \rho_{f_{CD}})g, 0, 0].$$

But

$$\rho_{f_{CD}} = \rho_0[1 - \beta(T_{CD} - T_0)],$$

$$\rho_f = \rho_0[1 - \beta(T_{CD} + T_p - T_0)].$$

Thus

$$\boldsymbol{G}_p = (-g\rho_0\beta T_p, 0, 0). \tag{13}$$

Taking the divergence of equation (12), and using the identity provided by equation (1), yields:

$$\nabla^2 P_p = g\rho_0\beta\frac{\partial T_p}{\partial x}. \tag{14}$$

Eliminating w_x between equations (11) and (12) results in

$$\frac{C_{p_f}\Delta T_0 K\rho_f}{\lambda_m L_x \mu}\left[\frac{\partial P_p}{\partial x} - g\rho_0\beta T_p\right] = \left[\frac{(\rho C_p)_m}{\lambda_m}\frac{\partial}{\partial t} - \nabla^2\right] T_p. \quad (15)$$

Furthermore, elimination of pressure between equations (14) and (15) yields:

$$\left[\frac{(\rho C_p)_m}{\lambda_m}\frac{\partial}{\partial t} - \nabla^2\right]\nabla^2 T_p + \frac{g\rho_0\beta C_{p_f}\Delta T_0 K\rho_f}{\lambda_m L_x \mu}\nabla_1^2 T_p = 0. \quad (16)$$

Equation (15) may be made dimensionless by defining:

$$t = \bar{t}\,.\,t^* = \frac{L_z^2(\rho C_p)_m}{\lambda_m}\bar{t}, \qquad x = L_x\bar{x},$$
$$y = L_y\bar{y}, \qquad z = L_z\bar{z}, \qquad T_p = \Delta T_0 \overline{T}_p.$$

The resulting equation is:

$$\left[\frac{\partial}{\partial \bar{t}} - \overline{\nabla}^2\right]\overline{\nabla}^2\overline{T}_p + A^2 R\overline{\nabla}_1^2\overline{T}_p = 0. \quad (17)$$

The Rayleigh number, R, is defined by:

$$R = \frac{g\rho_0\beta C_{p_f}\Delta T_0 L_x K\rho_f}{\lambda_m \mu}. \quad (18)$$

Aside from minor variations, equation (17) is essentially the same equation developed by a number of investigators (Lapwood [5], Combarnous [15]).

(b) *Nonlinear equations*

The solution to the linearized equations provide considerable insight into establishing the critical Rayleigh number, but the nonlinear equations have to be solved to predict behaviour beyond the onset of convective motion. The obvious procedure of solving equations (1)–(3) requires the substitution of equation (3) into equation (1) and the subsequent simultaneous solution of the resulting equation with equation (2). This formulation results in two partial differential equations with pressure and temperature as dependent variables. It will subsequently be referred to as the pressure solution.

An alternative method was proposed by Aziz and Hellums [12]. They employed a vector potential, the three-dimensional analog of the stream function in the solution of the Navier–Stokes equations. They had previously observed that this formulation was computationally superior to the pressure formulation. Numerical experiments indicated that the computer time required for the pressure solution was an order of magnitude higher than for the stream function solution for this problem also.

Thus following the approach of Aziz and Hellums [12], pressure is eliminated from equation (3) by taking the curl of the equation,

$$\boldsymbol{\Xi} = \nabla \times \boldsymbol{w} = -\frac{K\rho_f}{\mu}\nabla \times (\nabla P + \boldsymbol{G}) \quad (19)$$

where $\boldsymbol{\Xi}$ is defined as the vorticity vector.

Since $\nabla \times \nabla P = 0$, equation (19) becomes

$$\boldsymbol{\Xi} = -\frac{K\rho_f}{\mu}\nabla \times \boldsymbol{G}. \quad (20)$$

A vector potential, $\boldsymbol{\psi}$, may be defined such that

$$\boldsymbol{w} = \nabla \times \boldsymbol{\psi}. \quad (21)$$

Hirasaki and Hellums [16] prove that a vector potential defined by equation (21) exists and is solenoidal if the velocity field is solenoidal. As the density is assumed constant (except where it contributes to buoyancy), equation (3) implies a solenoidal velocity field, i.e.

$$\nabla\,.\,\boldsymbol{\psi} = 0. \quad (22)$$

With the aid of equation (22), it can be shown that

$$\boldsymbol{\Xi} = -\nabla^2\boldsymbol{\psi} = -\frac{K\rho_f}{\mu}\nabla \times \boldsymbol{G} \quad (23)$$

and

$$\nabla\,.\,\boldsymbol{w} = \nabla\,.\,(\nabla \times \boldsymbol{\psi}) = 0 \quad (24)$$

The no-flow boundary conditions restated in

terms of the vector potential are (Hirasaki and Hellums [16]):

$$\frac{\partial \psi_1}{\partial x} = \psi_2 = \psi_3 = 0 \qquad \text{at } x = 0, L_x \tag{25}$$

$$\frac{\partial \psi_2}{\partial y} = \psi_1 = \psi_3 = 0 \qquad \text{at } y = 0, L_y \tag{26}$$

$$\frac{\partial \psi_3}{\partial z} = \psi_1 = \psi_2 = 0 \qquad \text{at } z = 0, L_z. \tag{27}$$

The previous equations may be made dimensionless by the following substitutions:

$$w_x = w_x^* \bar{w}_x, \qquad x = L_x \bar{x} \tag{28}$$

$$w_y = w_y^* \bar{w}_y = \frac{L_y w_x^*}{L_x} \bar{w}_y, \qquad y = L_y \bar{y}$$

$$w_z = w_z^* \bar{w}_z = \frac{L_z w_x^*}{L_x} \bar{w}_z, \qquad z = L_z \bar{z}$$

$$\psi_1 = \frac{L_y L_z}{L_x} w_x^* \bar{\psi}_1$$

$$\psi_2 = L_z w_x^* \bar{\psi}_2$$

$$\psi_3 = L_y w_x^* \bar{\psi}_3.$$

Equations (25)–(27) may now be made dimensionless to give:

$$\bar{w}_x = \frac{\partial \bar{\psi}_3}{\partial \bar{y}} - \frac{\partial \bar{\psi}_2}{\partial \bar{z}} \tag{29}$$

$$\bar{w}_y = \frac{\partial \bar{\psi}_1}{\partial \bar{z}} - \frac{\partial \bar{\psi}_3}{\partial \bar{x}} \tag{30}$$

$$\bar{w}_z = \frac{\partial \bar{\psi}_2}{\partial \bar{x}} \quad \frac{\partial \bar{\psi}_1}{\partial \bar{y}}. \tag{31}$$

Furthermore by defining:

$$T = T_0 + \Delta T_0 \cdot \bar{T} \tag{32}$$

$$w_x^* = \frac{\lambda_m}{L_z C_{p_f}} \tag{33}$$

and assuming that

$$\rho_f = \rho_0 (1 - \beta \Delta T_0 \bar{T}) \tag{34}$$

the dimensionless form of equation (23) may be obtained:

$$\bar{\nabla}^2 \bar{\psi}_1 = B^2 R \cos\theta \frac{\partial \bar{T}}{\partial \bar{y}} \tag{35}$$

$$\bar{\nabla}^2 \bar{\psi}_2 = -AR \left[\sin\theta \frac{\partial \bar{T}}{\partial \bar{z}} + A \cos\theta \frac{\partial \bar{T}}{\partial \bar{x}} \right] \tag{36}$$

$$\bar{\nabla}^2 \bar{\psi}_3 = AB^2 R \sin\theta \frac{\partial T}{\partial \bar{y}}. \tag{37}$$

The dimensionless form of the boundary conditions would be:

$$\frac{\partial \bar{\psi}_1}{\partial \bar{x}} = \bar{\psi}_2 = \bar{\psi}_3 = 0 \text{ at } \bar{x} = 0, 1 \tag{38}$$

$$\frac{\partial \bar{\psi}_2}{\partial \bar{y}} = \bar{\psi}_1 = \bar{\psi}_3 = 0 \text{ at } \bar{y} = 0, 1 \tag{39}$$

$$\frac{\partial \bar{\psi}_3}{\partial \bar{z}} = \bar{\psi}_1 = \bar{\psi}_2 = 0 \text{ at } \bar{z} = 0, 1. \tag{40}$$

The energy equation [equation (2)] may be made dimensionless by similar substitutions to yield:

$$\bar{\nabla}^2 \bar{T} - A \left\{ \bar{w}_x \frac{\partial \bar{T}}{\partial \bar{x}} + \bar{w}_y \frac{\partial \bar{T}}{\partial \bar{y}} + \bar{w}_z \frac{\partial \bar{T}}{\partial \bar{z}} \right\} = \frac{\partial \bar{T}}{\partial \bar{t}} \tag{41}$$

with an initial condition of:

$$\bar{T}(\bar{x}, \bar{y}, \bar{z}, 0) = f(\bar{x}, \bar{y}, \bar{z}), \quad \text{normally} = 0 \tag{42}$$

and boundary conditions of:

$$\bar{T} = 1{\cdot}0 \text{ at } \bar{x} = 0 \tag{43}$$

$$\bar{T} = \ 0 \text{ at } \bar{x} = 1{\cdot}0 \tag{44}$$

$$\frac{\partial \bar{T}}{\partial \bar{y}} = 0 \text{ at } \bar{y} = 0, 1; \frac{\partial \bar{T}}{\partial \bar{z}} = 0 \text{ at } \bar{z} = 0, 1. \tag{45}$$

It will be noted that as $L_y \to \infty$, the aspect ratio B approaches 0, which would result in $\bar{\psi}_1$ and $\bar{\psi}_3$ to be equal to 0 at all times [from equations (35) and (37)], which would mean that $\bar{w}_y = 0$ at all times, and the two-dimensional problem is approached. In this case $\bar{\psi}_2$ would be the conventional stream function. For $\theta = 90$, the horizontal case, equation (35) indicates $\bar{\psi}_1$ to be equal to zero at all times. This situation was the only case investigated numerically. The formula-

tion was obtained considering any angle of inclination to make it more general.

3. METHOD OF SOLUTION

(a) *Linearized equations*

Following the approach of Lapwood [5], Karra [9] and numerous other investigators, the solution to the linearized equations is assumed to be of the form:

$$\bar{T}_p = E \sin l\pi\bar{x} \quad \cos m\pi\bar{y} \cos \pi\bar{z}\, e^{\eta t}. \qquad (46)$$

The integers l, m and n are the wave numbers of the disturbance. It is easily seen that the point of neutral stability is attained when $\eta = 0$. For a positive η, any disturbance will grow with time, whereas for a negative η, any disturbance will decay with time.

Substitution of equation (46) (with $\eta = 0$) into equation (17) yields:

$$-(l^2\pi^2A^2 + m^2\pi^2B^2 + n^2\pi^2) \times (A^2\pi^2l^2 + B^2\pi^2m^2 + n^2\pi^2) + A^2R_c(B^2\pi^2m^2 + n^2\pi^2) = 0 \qquad (47)$$

or

$$R_c = \frac{\pi^2(l^2A^2 + m^2B^2 + n^2)^2}{A^2(B^2m^2 + n^2)}. \qquad (48)$$

Equation (48) is essentially the same relationship as obtained by Lapwood. (The identity between the relationships is obtained by letting $A = B = 1$.) Assuming B to be 0 yields the relationship given by Karra [9]. Equation (48) may now be employed to give the critical Rayleigh number as a function of the wave numbers for a number of aspect ratios. The results obtained are presented in Section 4.

(b) *Nonlinear equations*

Present day mathematical knowledge does not allow in general the solution of nonlinear partial differential equations in an analytical form. Numerical techniques are necessary at one stage or another. In early investigations, Wooding [6, 17] perturbed the original equations and then solved the perturbation equations numerically. Subsequent investigators solved the basic equations numerically. As the perturbation solution is limited to low Rayleigh numbers, the equations as presented under Mathematical Formulation were solved numerically in this investigation. The numerical methods are well known (e.g. Varga [18]), and only a brief outline is given here. The algorithms employed are defined in Appendix 1.

The numerical solution is obtained by dividing the domain of interest into a grid network such that $\bar{x}_i = (i-1)\Delta\bar{x}$, $\bar{y}_j = (j-1)\Delta\bar{y}$ and $\bar{z}_k = (k-1)\Delta\bar{z}$ (this definition is employed to be compatible with the computer program where the subscript 0 is not allowed). The partial differential equations are also discretized according to standard procedures. The energy equation was solved by the Alternative Direction Implicit (ADI) procedure. A form convenient for the problem under consideration is given by Aziz [3]. It may be regarded as a perturbation of the form first proposed by Douglas [19]. (The solution algorithm is given in Appendix 1.) The nonlinearities (mass fluxes) in the equation were linearized over a time step. The assumed value was taken to be the arithmetic average of the mass flux at the beginning of the time step and the end of the time step. (As the value at the end

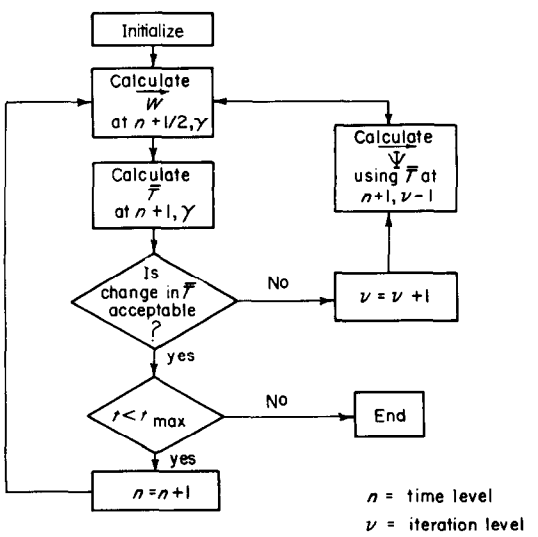

FIG. 2. Simplified flow diagram of the computer program.

of the time step is not known, this procedure implies iteration at a time step.)

The equation of motion was solved by the method of Successive Over-Relaxation (SOR). The solution algorithm is well known, and is given for the convenience of the reader in Appendix 1.

The two equations were then solved simultaneously by the algorithm presented in Fig. 2.

4. RESULTS AND DISCUSSION OF RESULTS

(a) *Linearized equations*

The critical Rayleigh numbers were obtained as a function of the wave numbers considering the aspect ratios of $A = 1$, $B = 1$; $A = 3$, $B = 3$; and $A = 3$, $B = 6$. The results are presented in Table 1. The two-dimensional flow regime, characterized by $m = 0$, yields critical Rayleigh numbers which are independent of B. The lowest critical Rayleigh number calculated is 39·47. This corresponds to the value of $4\pi^2$ obtained by Lapwood [5].

Table 1 may also be rearranged to yield the number of possible solutions for each value of the Rayleight number. For instance at a Rayleigh number of 60, linear theory predicts 9 possible solutions for the confined porous medium of aspect ratios $A = 3$, $B = 3$. Of these 9 solutions, 4 predict the motion to be two-dimensional. If the aspect ratios are changed to $A = 3$, $B = 6$, only two-dimensional motion would be possible for the same Rayleigh number. At low Rayleigh numbers (near the critical) the table suggests that two-dimensional motion is preferred. The motion may thus be described to be in the form

Table 1. Linear theory: critical Rayleigh number vs. wave numbers

l	m	n	R_c $A=1, B=1$	R_c $A=3, B=3$	R_c $A=3, B=6$
1	0	1	39·47	109·65	109·65
		2	61·68	46·32	46·32
		3		39·47	39·47
		4		42·83	42·83
		5		50·70	50·70
		6		61·68	61·68
1	1	1	44·41	39·58	62·71
		2	71·05	40·82	65·82
		3		44·41	71·05
		4		50·70	78·46
		5		59·63	88·08
		6		71·05	

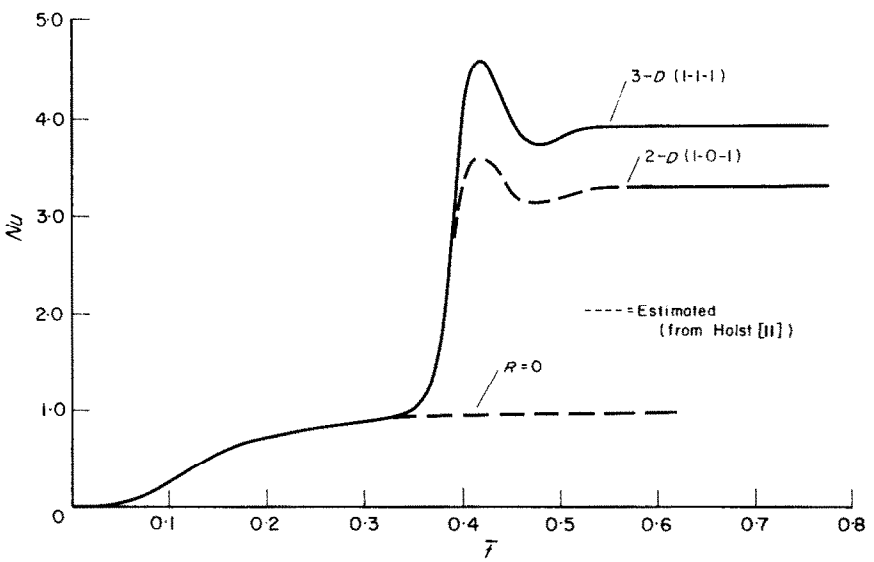

FIG. 3. Transient heat transfer at the cold boundary, $R = 120$, $A = 1, B = 1$.

Table 2. Summary of steady state results

R	A	B	l	m	n	Nu	$\bar{\psi}_{2\,min}$	$\bar{\psi}_{2\,max}$	$\bar{\psi}_{3\,min}$	$\bar{\psi}_{3\,max}$
120	1	1	1	1	1	3·94	−5·26	5·02	− 5·17	5·11
	1	1	1	0	1	3·49	−6·30	0	0	0
	3	3	1	1	1	3·57	−4·73	4·73	−19·07	19·09
	3	3	1	0	3	3·49	−6·30	0	0	0
	3	6	1	1	1	2·98	−1·52	1·52	−21·60	21·55
	3	6	1	0	3	3·49	−6·30	0	0	0
60	1	1	1	1	1	1·67	−2·05	2·00	− 2·03	2·01
	1	2	1	0	1	1·89	−3·01	0·01	− 0·00004	0·00004

of rolls with axes of the rolls parallel to the shorter sides. These observations are analogous to those presented by Davis [20] for the open cavity. At sufficiently high Rayleigh numbers, this conclusion may no longer be valid and another solution may be preferred. This change from one mode to another has been observed by Combarnous [15] in the form of cyclic changes in the heat transfer characteristics.

(b) *Nonlinear equations*

The transient 3-D solution is presented in Fig. 3. The figure indicates that the 3-D motion represents a significant increase in the heat transfer across the porous medium when compared to the 2-D motion. The solution shown has wave numbers of $l = 1$, $m = 1$ and $n = 1$. According to the linear theory this particular solution has a critical Rayleigh number of 44·41 which is higher than the critical Rayleigh number of the 2-D (roll) solution. Table 2 presents a summary of important numerical results obtained with the numerical method described earlier. The table shows that at a Rayleigh number of 120 the 1–1–1 solution exhibits considerably more heat transfer than the

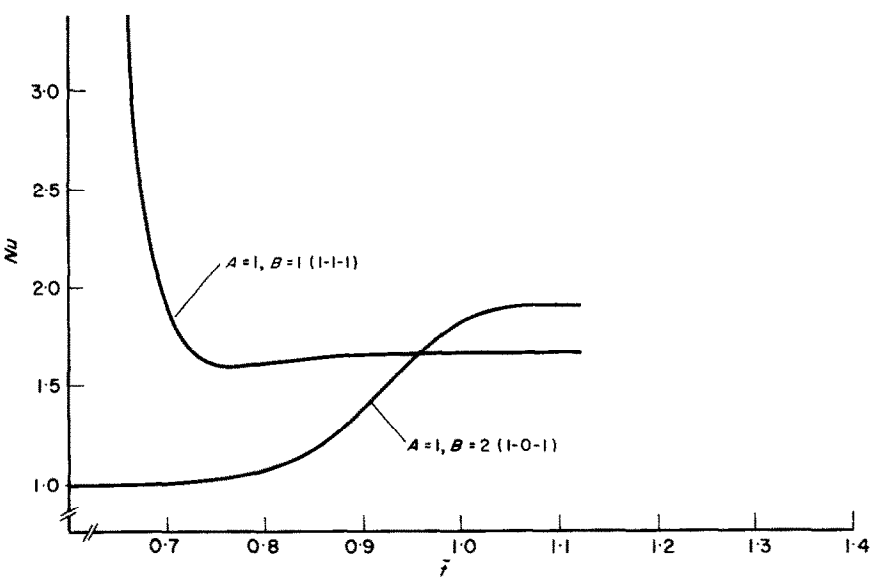

FIG. 4. Transient heat at the cold boundary, $R = 60$, $\theta = 90$ ($A = 1$, $B = 1$ solution is started with the steady state $R = 120$ solution: $A = 1$, $B = 2$ solution is started with steady state conduction solution).

1–0–1 solution. Using criterion of Platzman [21], whereby the solution exhibiting the maximum heat transfer is physically preferred, the 1–1–1 solution would be preferred at a Rayleigh number of 120. At lower Rayleigh numbers, as will be shown subsequently, the situation is reversed. It should be noted at this time that no analysis of the effect of grid spacing on the 3-D solution has been carried out due to the extremely high computer time requirements. On this basis the value of the Nusselt number might be in error by as much as 18 per cent (based on 2-D studies conducted by Holst [11]). However, the difference between the two solutions is of considerable magnitude and both solutions were obtained for similar grid sizes. The conclusion that the (1–1–1) solution would be physically preferred is consequently reasonable.

Subsequent results (see Table 2) obtained by changing the aspect ratios without changing the grid spacing are somewhat suspect. The solutions were obtained by using the steady state $A = 1$, $B = 1$ solution as the initial condition. According to the linear theory, the results obtained are possible. The proximity of the steady state Nusselt numbers, combined with the coarse grid system employed in developing the $A = 3$, $B = 3$ case, do not allow the determination of the physically most likely convection pattern (1–1–1 or 1–0–3 are the only two alternatives investigated; the absolute optimum may very well be a pattern not investigated). The results obtained for the $A = 3$, $B = 6$ case definitely suggest the 1–0–3 (3 cell, 2-D) mode to be more likely in a physical application.

As a number of experimental results were obtained at a Rayleigh number of approximately 60 (Holst [11]), an investigation of the effect of the third dimension at that Rayleigh number seemed appropriate. Two situations were investigated: the first assumed $A = 1$, $B = 1$ and employed the steady state 1–1–1 solution at $R = 120$ as the initial condition, the second case assumed $A = 1$, $B = 2$ and employed the steady state conduction solution as the initial condition. The transient results thus obtained are presented in Fig. 4. The situation where $A = 1$, $B = 2$ essentially duplicated the results obtained by a 2-D model (Holst [11]). The minor variations between the solutions were

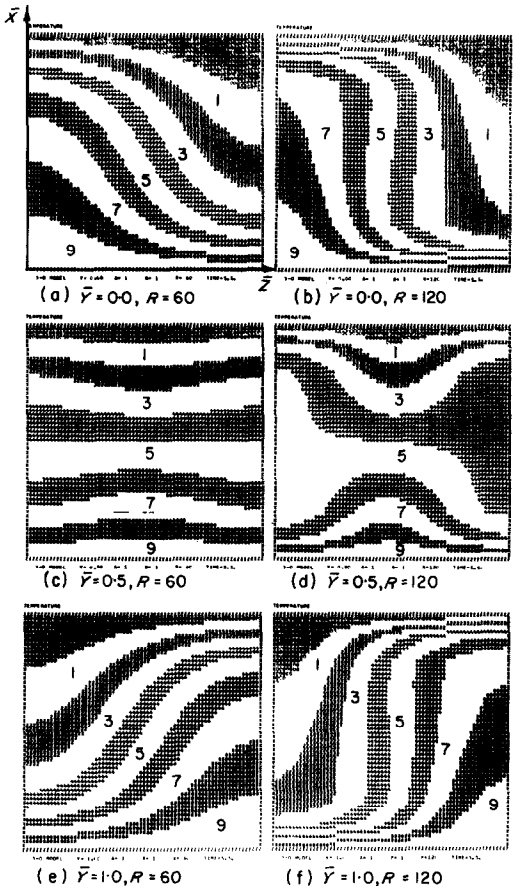

FIG. 5. Steady state temperature distributions. $A = 1$, $B = 1$.

believed to be attributable to the slightly different spacings employed. The two-dimensional form of the solution was predicted by the linear theory and provides an excellent check on the consistency of the two computer models. The (1–1–1) solution obtained for $A = 1$, $B = 1$ is of interest, as it suggests that at this low Rayleigh number the 2-D one cell solution is physically more likely. This represents a different preferred mode than that obtained at $R = 120$.

Figure 5† shows a comparison of the steady state temperature distributions for $R = 60$ and 120 at $\bar{y} = 0$, 0·5 and 1·0. All contour maps shown on this figure are for $A = 1$ and $B = 1$. Figure 6 presents a similar comparison for the

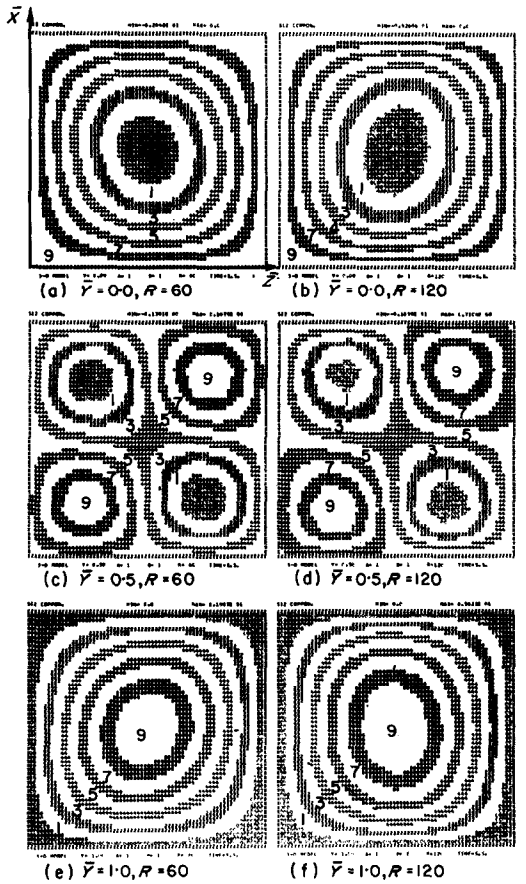

FIG. 6. Steady state $\bar{\psi}_2$ distributions, $A = 1$, $B = 1$.

ψ_2 component of the vector potential. Figures 7 and 8 presents a comparison of temperature and ψ_3 distribution at $R = 120$ for the cases $A = 3$, $B = 3$ and $A = 3$, $B = 6$. The $\bar{\psi}_3$ distributions are notably missing for the planes $\bar{y} = 0$ and $\bar{y} = 1·0$ in Fig. 8 due to the fact that the boundary conditions specify them to be zero at these locations. In other words, the flow is two-dimensional at the boundaries. From the temperature maps it is apparent that the mid-plane temperature distributions do not resemble the two-dimensional results. The temperature

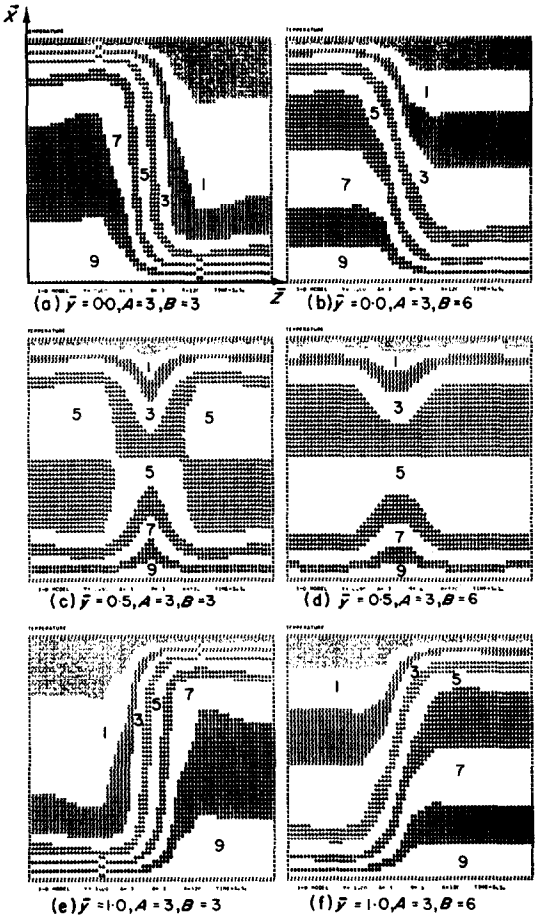

FIG. 7. Steady state temperature distributions, $R = 120$.

distributions obtained at the bounding surfaces are notably similar to the 2-D results. This is to be expected, as the flow at these surfaces is strictly two-dimensional. Considering the possible directions of circulation at the opposing surfaces (e.g. at $\bar{y} = 0$ and $\bar{y} = 1·0$), only two alternatives are present. If they are the same,

† The contour maps are constructed on the line printer by a program which divides the range of a two-dimensional array into 10 subranges. Each subrange is then filled by a special character. The first subrange is filled by a 0, the second by a blank, the third by a 2, etc., ending with a blank in the 10th subrange. To aid in the interpretation the blanks are coded with the number they should contain.

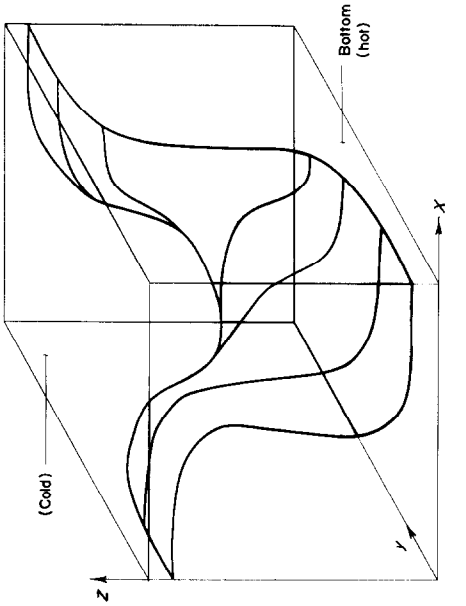

FIG. 9. Isometric projection of $\bar{T} = 0{\cdot}5$ surface, $R = 120$.

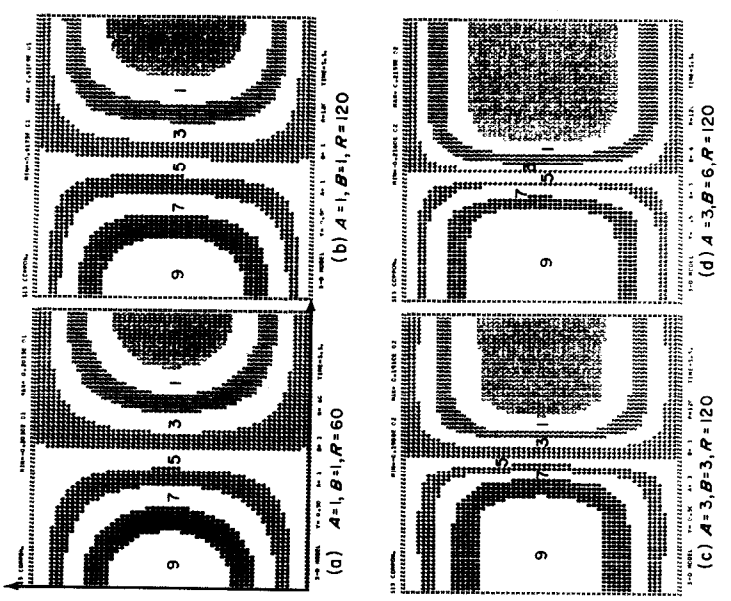

FIG. 8. Steady state $\bar{\psi}_3$ distributions, $\bar{y} = 0{\cdot}5$.

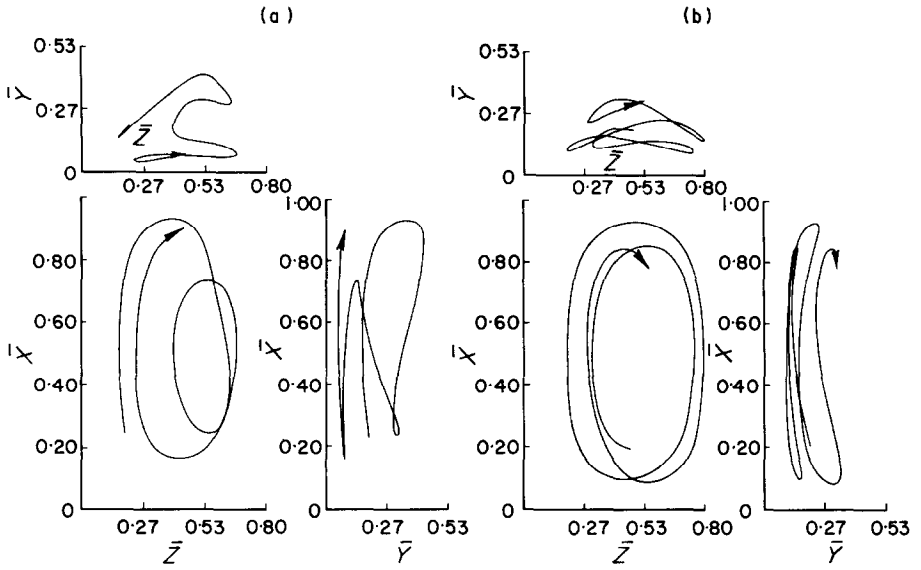

FIG. 10. Streak line, $R = 120$, $A = 1$, $B = 1$.

two-dimensional motion is the most probable result for the aspect ratios and Rayleigh numbers considered here. If they are different, the solutions presented in Figs. 5–13 are most likely. The possible solutions may be obtained using equation (48). The 1–1–1 solution requires that the maps at the opposing bounding surfaces be mirror images of each other. Figures 5–7 comply with this requirement.

Referring to Figs. 5–8, it is difficult to visualize the fluid movement when the flow is three-dimensional. Some attempts have been made to

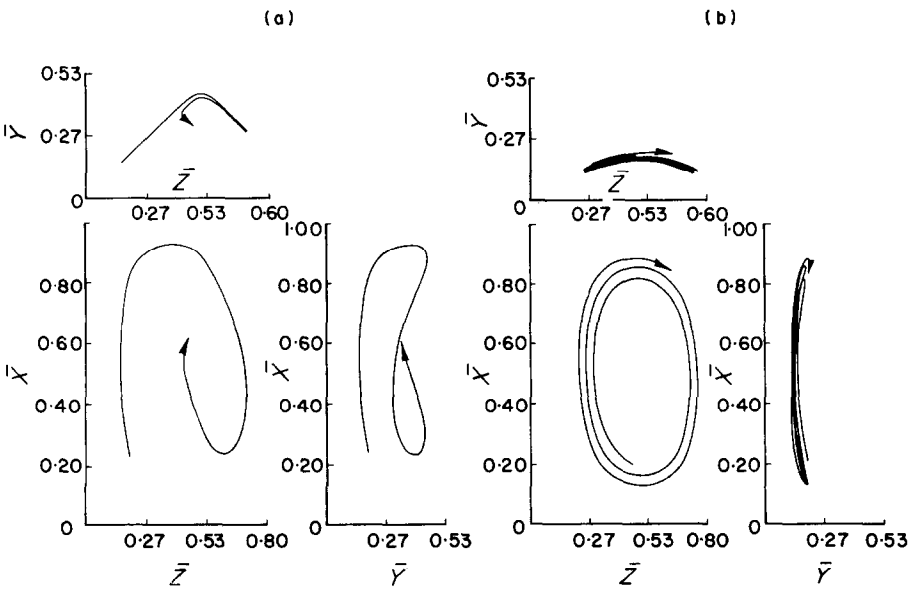

FIG. 11. Streak line, $R = 60$, $A = 1$, $B = 1$.

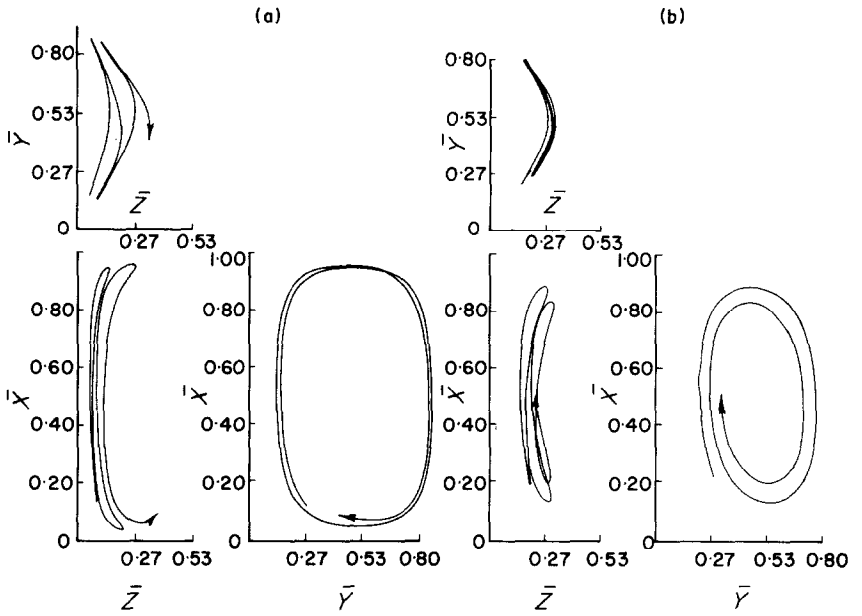

FIG. 12. Streak line, $R = 60, A = 1, B = 1$.

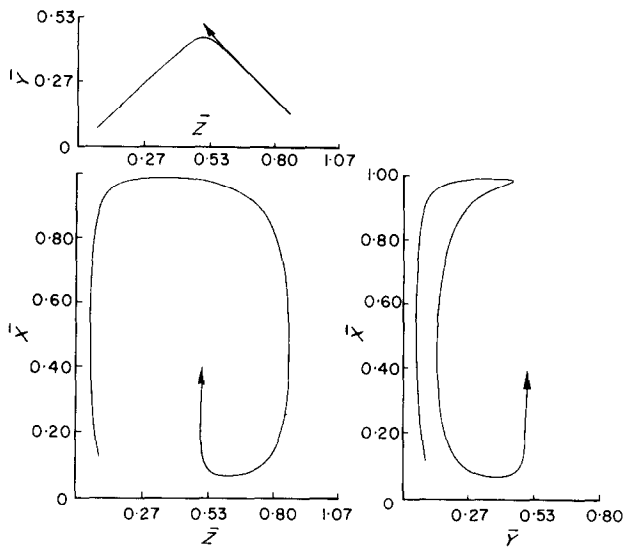

FIG. 13. Streak line, $R = 60, A = 1, B = 1$.

aid in the visualization. Figure 9 represents the first attempt by presenting isometric projections of the $\bar{T} = 0{\cdot}5$ isothermal surface. For the $A = 3, B = 3$ case the motion may be described by two counter rotating rolls with a mixing zone in the middle. Visualization of the flow in the mixing zone is somewhat more difficult. To aid in the interpretation of the flow in this mixing zone a program was developed to trace the path of a fluid particle. Figure 10(a) is the streakline

obtained for a particle originally at the location $\bar{x} = 0{\cdot}2$, $\bar{y} = 0{\cdot}2$ and $\bar{z} = 0{\cdot}2$. The streakline is presented by a top, front, and side view. There is no clear circulating pattern evident, suggesting that the velocities were too large for the grid system considered in order for this method to yield easily interpretable results. Figure 10(b) presents similar results for a fluid originally located at $\bar{x} = 0{\cdot}2$, $\bar{y} = 0{\cdot}2$ and $\bar{z} = 0{\cdot}5$. The streakline for this particle indicates the flow to be more or less two-dimensional in the $\bar{x}$–$\bar{z}$ plane.

Similar results obtained for $A = 1$, $B = 1$ and $R = 60$ are presented in Figs. 11–13. As the fluid was moving at lower velocities, the results are more accurate. The general circulating pattern is similar to that obtained at a Rayleigh number of 120.

As is evident from the isometric projections and streakline figures, the cellular motion is not very easily visualized or described. Further investigations would have to be performed to obtain an estimate of the signal-to-noise ratio in the solution: that is, how much of the apparent randomness is due to the method of tracing the particle and how much is actual physical behaviour. To carry out this type of investigation in depth, the grid spacing would have to be altered. This would require more computer time than was available for this investigation. Decreasing the Rayleigh number has a similar effect however. On this basis, it can be seen that the randomness in the streaklines for $R = 120$ is primarily due to inaccuracies in the solution, and the streaklines obtained for $R = 60$ provide a better picture of the circulating pattern.

CONCLUSIONS

1. Three-dimensional motion may under certain instances result in higher heat transfer across the porous medium, depending upon the physical dimensions of the medium and the Rayleigh number of the system.

2. The critical Rayleigh numbers obtained from the linear theory provide considerable insight into the physical mode of convection at Rayleigh numbers above the critical.

3. As two-dimensional solutions always satisfy the three-dimensional equations, there is an inherent multiplicity in the solution if three-dimensional motion is possible.

4. The method of using the vector potential in the formulation yielded entirely acceptable results. It is the authors' belief that this formulation is superior to the one using pressure as one of the dependent variables.

ACKNOWLEDGEMENTS

This research was supported by the National Research Council of Canada and the Petroleum Education Aid Fund of Alberta. One of the authors, P. H. Holst, was on a Shell Canada Centennial Fellowship during the course of this investigation. All computations were performed on the IBM 360/50 computer at The University of Calgary.

REFERENCES

1. Lord RAYLEIGH, On convection currents in a horizontal layer of fluid, when the higher temperature is on the underside. *Phil. Mag. Ser.* 6, **32**, 529–546 (1961).
2. S. CHANDRASEKHAR, *Hydrodynamic and Hydromagnetic Stability*. Clarendon Press (1961).
3. K. AZIZ, A numerical study of cellular convection, Ph.D. thesis, Rice University (1965).
4. P. H. ROBERTS, On non-linear Bénard convection, *Non-Equilibrium Thermodynamics. Variational Techniques and Stability*. edited by R. J. DONNELLY, R. HERMAN and I. PRIGOGINE. University of Chicago Press (1965).
5. E. R. LAPWOOD, Convection of a fluid in a porous medium. *Proc. Camb. Phil. Soc.* **44**, 508–521 (1968).
6. R. A. WOODING, Steady state free thermal convection of liquid in a saturated permeable medium, *J. Fluid Mech.* **2**, 273–285 (1957).
7. J. W. ELDER, Steady free convection in a porous medium heated from below, *J. Fluid Mech.* **27**, 29–48 (1967).
8. J. W. ELDER, Transient convection in a porous medium, *J. Fluid Mech.* **27**, 609–623 (1967).
9. P. S. KARRA, A numerical study of natural convection in porous media, M.Sc. thesis, The University of Calgary (1968).
10. B. K. CHAN, C. M. IVEY and J. M. BARRY, Natural convection in enclosed porous media with rectangular boundaries, *J. Heat Transfer* **89**, 295–299 (1970).
11. P. H. HOLST, A theoretical and experimental investigation of natural convection in porous media, Ph.D. thesis, The University of Calgary (1970).
12. K. AZIZ and J. D. HELLUMS, Numerical solution of the three dimensional equations of laminar natural convection, *Physics Fluids* **10**, 314–324 (1967).
13. P. H. HOLST and K. AZIZ, A numerical study of natural convection in a confined porous medium with temperature dependent properties, submitted for publication.
14. M. PRATS, The effect of horizontal fluid flow on thermally induced convection currents in porous mediums, *J. Geophys. Res.* **71**, 4835–4838 (1966).

15. M. COMBARNOUS, Convection naturelle et convection mixte en milieu poreux, Thèse Université de Paris, Edition Techniq., Inst. Francais du Pétrole (1970).
16. G. J. HIRASAKI and J. D. HELLUMS, A general formulation of the boundary conditions on the vector potential in three-dimensional hydrodynamics, *Q. Appl. Math.* **16**, 331 (1968).
17. R. A. WOODING, An experiment on free thermal convection of water in a saturated permeable medium, *J. Fluid Mech.* **3**, 582–599 (1958).
18. R. S. VARGA, *Matrix Iterative Analysis*. Prentice-Hall (1962).
19. J. DOUGLAS, Alternating direction methods for three space variables, *Num. Math.* **4**, 41–63 (1962).
20. S. H. DAVIS, Convection in a box: linear theory, *J. Fluid Mech.* **30**, 465–478 (1967).
21. G. W. PLATZMAN, The spectral dynamics of laminar convection, *J. Fluid Mech.* **23**, 481–510 (1965).
22. D. M. YOUNG, Iterative methods for solving partial differential equations of elliptic type, *Trans. Am. Math. Soc.* **76**, 92–111 (1954).
23. D. W. PEACEMAN and H. RACHFORD JR., The numerical solution of parabolic and elliptic equations. *J. Soc. Ind. Appl. Math.*. **3**, 28 (1955).

APPENDIX 1

Numerical Methods

1. *Elliptic equation*

The equation of motion [equations (35)–(37)] was arranged in the form of an elliptic equation and solved by the method of Successive Over-Relaxation (SOR) in the majority of the solutions presented. The procedure is well established (e.g. Young [22]) and only a very brief description follows. The algorithm is presented for the following general equation:

$$A^2\frac{\partial}{\partial\bar{x}}\left(\frac{\partial\bar{\psi}}{\partial\bar{x}}\right)+B^2\frac{\partial}{\partial\bar{y}}\left(\frac{\partial\bar{\psi}}{\partial\bar{y}}\right)+\frac{\partial}{\partial\bar{z}}\left(\frac{\partial\bar{\psi}}{\partial\bar{z}}\right)+d=0 \qquad (A.1)$$

where d is a function of x, y and z.

The $\bar{\psi}$ distribution was obtained by discretizing the three space dimensions and subsequently calculating $\bar{\psi}$ values at every grid point by iteration. Thus at time $n+1$

$$\bar{\psi}^{v+1}_{i,j,k}=(1-\omega)\bar{\psi}^{v}_{i,j,k}+\frac{\omega}{C}\left\{\frac{A^2}{\Delta\bar{x}^2}\left(\bar{\psi}^{v+1}_{i-1,j,k}+\bar{\psi}^{v}_{i+1,j,k}\right)+\frac{B^2}{\Delta\bar{y}^2}\left(\bar{\psi}^{v+1}_{i,j+1,k}+\bar{\psi}^{v}_{i,j+1,k}\right)+\frac{1}{\Delta\bar{z}^2}\left(\bar{\psi}^{v+1}_{i,j,k-1}+\bar{\psi}^{v}_{ij,k+k}\right)+d_{i,j,k}\right\} \qquad (A.2)$$

where

$$C=\frac{2A^2}{\Delta\bar{x}^2}+\frac{2B^2}{\Delta\bar{y}^2}+\frac{2}{\Delta\bar{z}^2} \qquad (A.3)$$

the subscripts i, j and k, and the grid spacing $\Delta\bar{x}$, $\Delta\bar{y}$ and $\Delta\bar{z}$ are defined such that: $\bar{x}_i=(i-1)\Delta\bar{x}$, $\bar{y}_j=(j-1)\Delta\bar{y}$ and $\bar{z}_k=(k-1)\Delta\bar{z}$. v is the iteration level.

The relaxation factor, ω, may be obtained by a method proposed by Young [22]. Thus

$$\omega=\frac{2}{1+\sqrt{1-\left(\frac{1}{\frac{1}{\Delta\bar{x}^2}+\frac{1}{\Delta\bar{y}^2}+\frac{1}{\Delta\bar{z}^2}}\left[\frac{1}{\Delta\bar{x}^2}\cos A\,\pi\Delta\bar{x}+\frac{1}{\nabla\bar{y}^2}\cos A\,\pi\Delta\bar{y}+\frac{1}{\Delta\bar{z}^2}\cos\pi\Delta\bar{z}\right]\right)}}. \qquad (A.4)$$

In this problem d takes the following values [see equations (35)–(37)]:

$$d=-B^2R\cos\theta\frac{\partial\bar{T}}{\partial\bar{y}}$$

$$d=AR\left[\sin\theta\frac{\partial\bar{T}}{\partial\bar{z}}+A\cos\theta\frac{\partial\bar{T}}{\partial\bar{x}}\right]$$

$$d=-AB^2R\sin\theta\frac{\partial\bar{T}}{\partial\bar{y}}.$$

Iteration of equation (A.2) was continued until the following criterion was met:

$$\frac{\max_{i,j,k}\left|\bar{\psi}^{v+1}_{i,j,k}-\bar{\psi}^{v}_{i,j,k}\right|}{\left|\bar{\psi}_{\min}\right|+\left|\bar{\psi}_{\max}\right|+0{\cdot}01}\leqslant\varepsilon.$$

The values of $|\bar{\psi}_{\min}|$ and $|\bar{\psi}_{\max}|$ were obtained from the previous time step. The value of ε was generally taken to be equal to 10^{-5}.

2. *Parabolic equation*

The energy equation was solved numerically by writing it in the form of a parabolic equation and using one form of the commonly used noniterative Alternating Direction Implicit (ADI) procedure. This procedure was first introduced by Peaceman and Rachford [23].

Using the ADI procedure, equation (41) is discretized spatially, and a first approximation, $\bar{T}^*$, of the solution at time $(n+1)\Delta t$ is obtained by:

$$\left(\Omega_x-\frac{2}{\Delta t}\right)\bar{T}^*_{i,j,k,n+1}=-\left(\Omega_x+2\Omega_y+2\Omega_z+\frac{2}{\Delta t}\right)\bar{T}_{i,j,k,n} \qquad (A.5)$$

A second approximation, $\bar{T}^{**}$, is obtained by:

$$\left(\Omega_y-\frac{2}{\Delta t}\right)\bar{T}^{**}_{i,j,k,n+1}=\Omega_y\bar{T}_{i,j,k,n}-\frac{2}{\Delta t}\bar{T}^*_{i,j,k,n+1}. \qquad (A.6)$$

The final solution is obtained by:

$$\left(\Omega_z - \frac{2}{\Delta\bar{t}}\right)\bar{T}_{i,j,k,n+1} = \Omega_z \bar{T}_{i,j,k,n} - \frac{2}{\Delta\bar{t}}\bar{T}^*_{i,j,k,n+1}. \quad \text{(A.7)}$$

The Ω operators are defined by:

$$\Omega_x \bar{T}^*_{i,j,k,n+1} = \frac{A^2}{\Delta\bar{x}^2}[\bar{T}^*_{i-1,j,k,n+1} - 2\bar{T}^*_{i,j,k,n+1} + T_{i+1,j,k,n+1}] - \frac{A}{2\Delta\bar{x}}\bar{w}_{xi,j,k,n+\frac{1}{2}}(\bar{T}^*_{i+1,j,k,n+1} - \bar{T}^*_{i-1,j,k,n+1} \quad \text{(A.8)}$$

$$\Omega_y \bar{T}_{i,j,k,n} = \frac{B^2}{\Delta\bar{y}^2}[\bar{T}_{i,j-1,k,n} - 2\bar{T}_{i,j,k,n} + \bar{T}_{i,j+1,k,n}] - \frac{A}{2\Delta\bar{y}}\bar{w}_{yi,j,k,n+\frac{1}{2}}(\bar{T}_{i,j+1,k,n} - \bar{T}_{i,j-1,kn}) \quad \text{(A.9)}$$

$$\Omega_z \bar{T}_{i,j,k,n} = \frac{1}{\Delta\bar{z}^2}[\bar{T}_{i,j,k-1,n} - 2\bar{T}_{i,j,k,n} + \bar{T}_{i,j,k+1,n}] - \frac{A}{2\Delta\bar{z}}\bar{w}_{zi,j,k,n+\frac{1}{2}}(\bar{T}_{i,j,k+1,n} - \bar{T}_{i,j,k-1,n}). \quad \text{(A.10)}$$

In the first step of the three-step procedure, equation (A.5) is solved implicitly for one $\bar{x}$-grid line at a time. In the second step, equation (A.6) is solved for one $\bar{y}$-grid line at a time, while in the third and final step, equation (A.7) is solved for one $\bar{z}$-grid line at a time.

CONVECTION NATURELLE TRIDIMENSIONNELLE TRANSITOIRE DANS UN MILIEU POREUX CONFINÉ

Résumé—Des recherches expérimentales sur la convection naturelle dans un milieu poreux confiné a montre que le mouvement peut être bidimensionnel ou tridimensionnel. Le mode de convection dépend de la configuration physique et du nombre de Rayleigh. Cet article traite des résultats théoriques obtenus par la méthode des différences finies appliquée aux équations qui décrivent la convection naturelle transitoire dans un milieu poreux. Les équations ont été rendues plus adaptées à une solution numérique en introduisant un potentiel vecteur qui peut être considéré comme l'homologue tridimensionnel de la fonction de courant.

Les résultats numériques indiquent que, sous certaines conditions, le mouvement tridimensionnel résulte de taux de transfert thermique significativement plus élevés que dans le cas bidimensionnel au même nombre de Rayleigh. La configuration de la convection tridimensionnelle est illustrée par des projections isométriques des surfaces isothermes et des lignes qui représentent la trajectoire d'une particule fluide. Les équations linéarisées sont résolues pour fournir une estimation du nombre de modes de convection possibles en fonction du nombre de Rayleigh.

INSTATIONÄRE DREIDIMENSIONALE FREIE KONVEKTION IN PORÖSEN MEDIEN ENDLICHER AUSDEHNUNG

Zusammenfassung—Experimentelle Untersuchungen der freien Konvektion in porösen Stoffen endlicher Ausdehnung haben gezeigt, dass die Bewegung zwei- oder dreidimensional sein kann. Die Art der Konvektionsbewegung hängt ab von der Anordnung der Poren und der Rayleighzahl. Diese Arbeit behandelt die theoretischen Ergebnisse, die mit Hilfe des Differenzenverfahrens aus den Gleichungen erhalten wurden, die die instationäre freie Konvektion in porösen Medien beschreiben. Die Gleichungen wurden

dimensionales Gegenstück zur Stromfunktion betrachtet werden kann.

Die numerischen Ergebnisse zeigen, dass unter bestimmten Bedingungen die dreidimensionale Bewegung bei gleichen Rayleighzahlen zu bedeutend höherem Wärmeübergang im porösen Stoff führt als die zweideimensionale Bewegung. Das Strömungsbild der dreidimensionalen Konvektionsbewegung wird veranschaulieht durch isomere Projektionen von isothermen Oberflächen und Streifenlinien, die den Weg der Flüssigkeitsteilchen kennzeichnen. Die linearisierten Gleichungen werden gelöst, um eine Abschätzung der Zahl der möglichen Konvektionsarten als Funktion der Rayleighzahl zu erreichen.

НЕСТАЦИОНАРНАЯ ТРЕХМЕРНАЯ ЕСТЕСТВЕННАЯ КОНВЕКЦИЯ В ОГРАНИЧЕННЫХ ПОРИСТЫХ СРЕДАХ

Аннотация—Экспериментальные исследования естественной конвекции в ограниченной пористой среде показали, что движение может быть двух-или трехмерным. Вид конвекции зависит от физической коифигурации и числа Релея. В данной работе рассматриваются теоретические результаты, полученные с помощью решения в конечных разностях уравнений, описывающих нестационарную естественную конвекцию в пористых средах. Уравнения были приведены к более удобному для численного решения виду, используя векторный потенциал, который можно рассматривать как трехмерную функцию, обратную функции тока.

Численные результаты показывают, что при определенных условиях в результате трехмерного движения получаются значительно большие скорости переноса тепла поперек пористой среды, нежели при двухмерном движении при том же значении уисла Релея. Конвективный характер трехмерного движения иллюстрируется изометрическими проекциями изотермических поверхностей и треками частиц жидкости. Для оценки ряда возможных конвективных конфигураций в зависимости от числа Релея решаются линеаризованные уравнения.